Retinol and retinol binding protein stabilize transthyretin via formation of retinol transport complex

Suk-Joon Hyung*[+], Stéphanie Deroo* and Carol V. Robinson*[¶]

** Department of Chemistry, Oxford University, South Parks Road, Oxford, OX1 3QY, UK*

[+] Current Address: University of Michigan, Department of Chemistry, 930 N. University, Ann Arbor, MI 48109-1055, USA

This supplementary information contains four figures and three tables.

Analysis of subunit exchange assay

The subunit exchange data was simulated to calculate the proportion of each tetramer as a function of time by varying a wide range of disassembly rate constants independently ($k_{d,mon}$ and $k_{d,dim}$). In order to estimate the degree of correlation between the simulated subunit exchange profile and the experimental data the root mean square deviation (RMSD) was evaluated according to the following formula, where $[TTR]_{simulated}$ is the simulated mole ratio of TTR and $[TTR]_{experimental}$ is the measured mole ratio of TTR at time t in seconds, and n is the number of data points.

$$RMSD(simulated, experimental) = \sqrt{\frac{1}{n}\sum_{t=1}^{t}([TTR]_{simulated,t} - [TTR]_{experimental,t})^2}$$

The set of rate constants with the minimum RMSD was obtained for each subunit exchange experiment in order to obtain the best fit between simulated and experimental data. The apparent disassembly rate constant ($k_{d,app}$) for TTR_4 was reported as a sum of the optimised disassembly rate constants $k_{d,dim}$ and $k_{d,mon}$.

An example of optimising the disassembly rate constants is demonstrated for a subunit exchange reaction between [^{12}C-^{14}N] TTR homotetramer and [^{13}C-^{15}N] TTR homotetramer (at 4 ^{o}C). The result shows that the RMSD is minimised when $k_{d,mon}$ and $k_{d,dim}$ are 4.23 x 10^{-5} $M^{-1}s^{-1}$ and 6.18 x 10^{-5} $M^{-1}s^{-1}$, respectively (Supp. Fig. 1a). A fit over the experimental data using the optimised disassembly rate constant shows a good agreement between the model and the experimental data (Supp. Fig. 1b). The disassembly rate constants were measured from triplicate data sets to give a standard deviation.

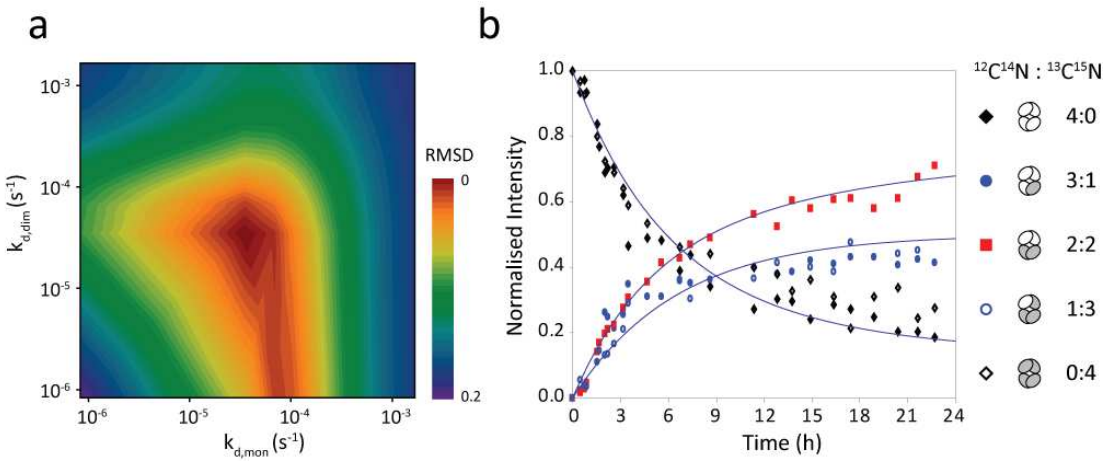

Supplementary Figure S1. Validation of the kinetic model for its ability to recapitulate the subunit exchange process.

a) Subunit exchange between [^{12}C-^{14}N] and [^{13}C-^{15}N] TTR homotetramers at 4 ^{o}C was simulated over 10,000 sets of $k_{d,mon}$ and $k_{d,dim}$. The RMSD between the model and the experimental data is smallest when $k_{d,mon}$ and $k_{d,dim}$ are 4.23 x 10^{-5} s^{-1} and 6.18 x 10^{-5} s^{-1}, respectively. b) The experimental data is shown with the subunit exchange profile predicted with the disassembly constants that minimise the RMSD.

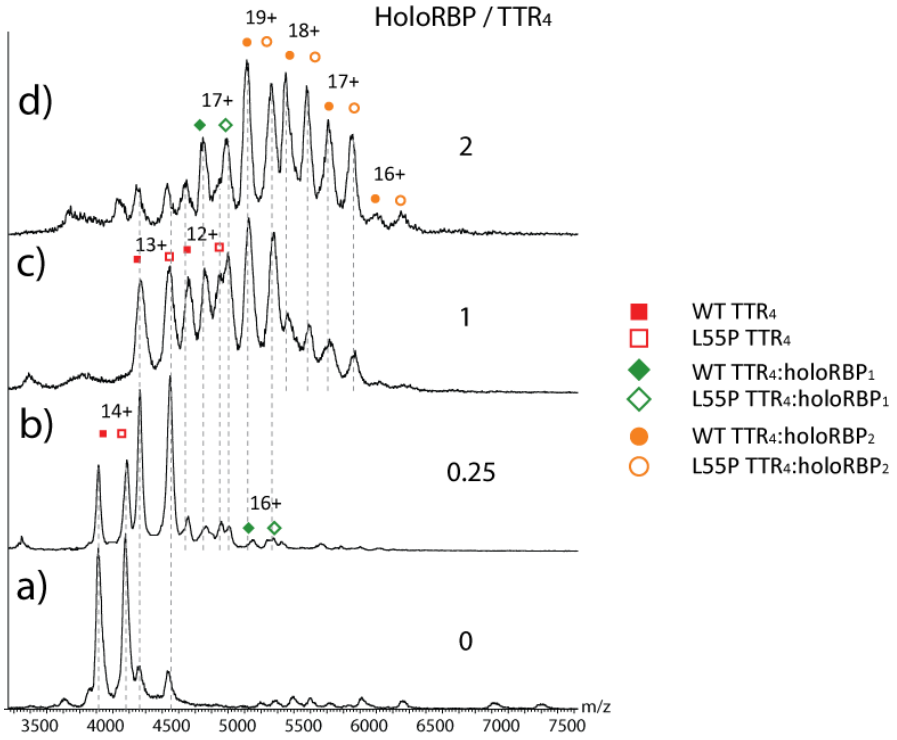

Supplementary Figure S2. Binding of variant and wild-type TTR to holoRBP.

Mass spectra of [^{12}C-^{14}N] WT and [^{13}C-^{15}N] L55P TTR_4 ($[TTR_4]_{Total}$ = 4.5 µM) incubated with holoRBP show similar affinity of RBP to both WT and L55P TTR. (a: control without RBP; b: 1.2 µM RBP; c: 4.5 µM RBP; d: 9µM RBP). The intensity of the peaks corresponding to the TTR and TTR in complex with one or two holoRBP is similar. Binding of RBP shifts the peaks to higher charge state due to the addition of a small amount of DMSO (< 1% v/v) from the retinol solution. At sub-stoichiometric, equimolar and excess amounts of holoRBP, the peaks corresponding to charge state series of WT TTR_4:$holoRBP_1$ complex are similar in abundance to those corresponding to the L55P TTR_4:$holoRBP_1$ complex (b-d). The results suggestthat the point mutations of TTR do not compromise the binding of RBP, consistent with that reported previously [1]. Similar result was obtained for V30M TTR.

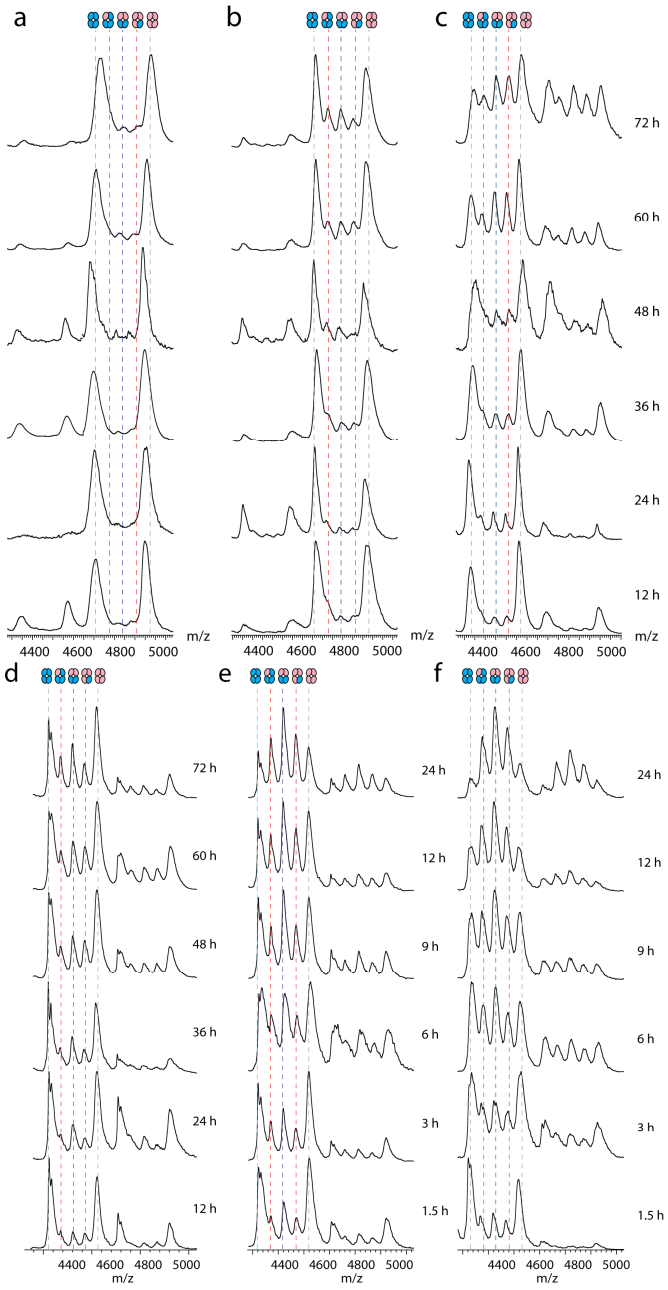

Supplementary Figure S3. Subunit exchange of variants of TTR.

Subunit exchange data of V30M [^{12}C-^{14}N]TTR and V30M [^{13}C-^{15}N]TTR with holoRBP (a), apoRBP (b), and without RBP (c). Analogous experiments with L55P [^{12}C-^{14}N]TTR and L55P [^{13}C-^{15}N]TTR are shown (d-f). Mass spectra acquired under dissociation MS conditions at fixed time intervals showing the depletion of homotetramers (4:0 and 0:4 tetramers in grey), and the formation of heterotetramers with a ratio of unlabelled to labelled monomers of 1:3 and 3:1 (red), and at 2:2 (blue) over time.

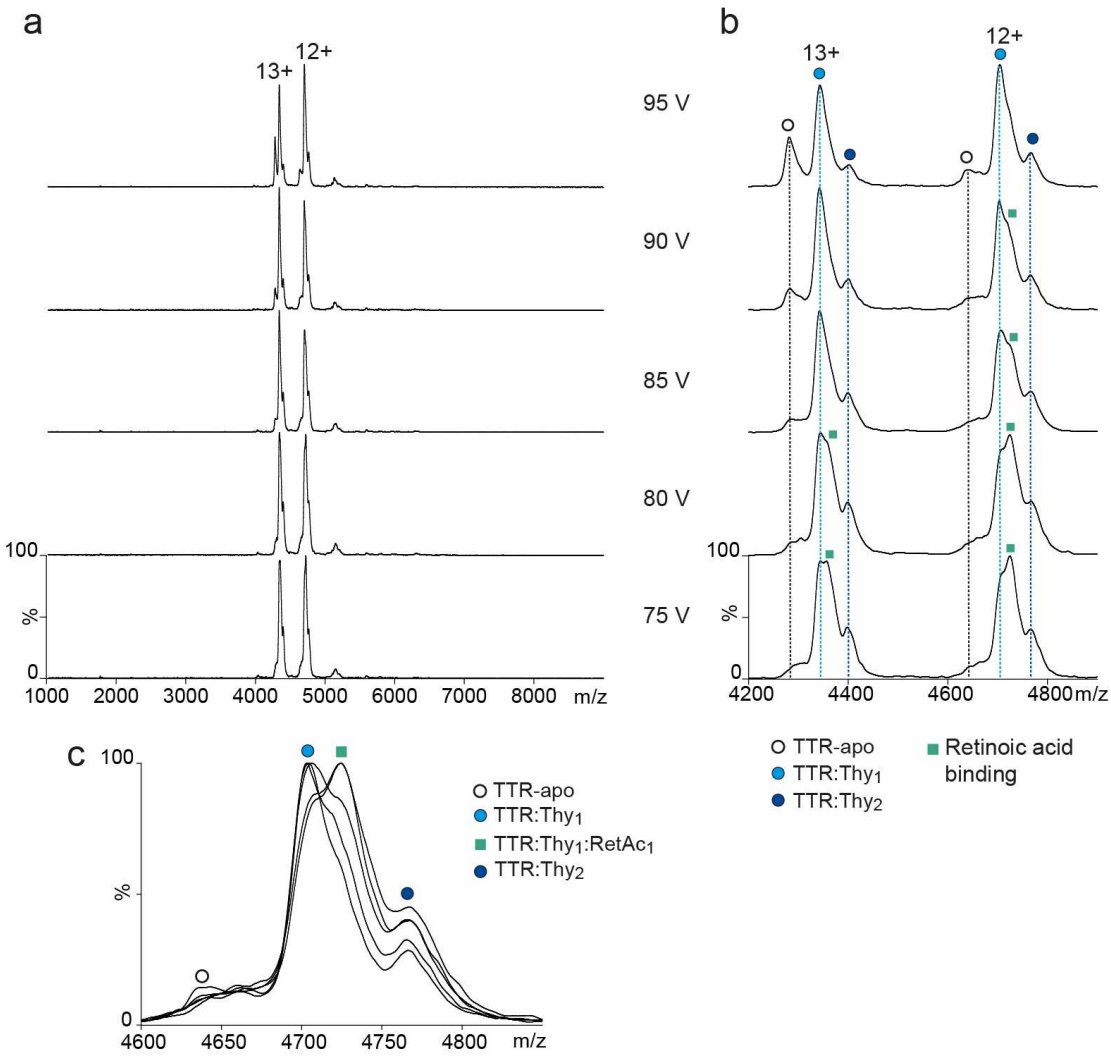

Supplementary Figure S4. Binding of retinoic acid and thyroxine.

(a) Mass spectra of TTR with a molar excess of thyroxine and retinoic acid (3-fold and 4-fold respectively) acquired under a range of MS conditions (cone voltage from 75 to 95 V). (b) A close-up of 13+ and 12+ charge states of TTR shows peaks corresponding to apoTTR (empty circle), TTR in complex with one and two thyroxine molecules (light and dark blue circle respectively), as well as TTR in complex with both thyroxine and retinoic acid (green square). (c) A close-up of 12+ charge state of TTR shows that retinoic acid binds to TTR:Thy_1 but not to TTR:Thy_2, suggesting its binding mode in the thyroxine binding channel.

Protein	Theoretical MW (Da)	Measured MW (Da)
[^{12}C-^{14}N] TTR	55570	55581 ± 5
[^{12}C-^{14}N] TTR:holoRBP$_1$	76599	76604 ± 21
[^{12}C-^{14}N] TTR:holoRBP$_2$	97628	98652 ± 38
[^{13}C-^{15}N] TTR	58685	58690 ± 6
[^{13}C-^{15}N] TTR:holoRBP$_1$	79714	79801 ± 25
[^{13}C-^{15}N] TTR:holoRBP$_2$	100742	100820 ± 43
holoRBP	20728	20731 ± 11

Supplementary Table S1. Theoretical and measured molecular masses of two RBP bound and 1 unbound state of TTR ([^{12}C-^{14}N] and [^{13}C-^{15}N] labelled forms) observed in Figure 1b.

TTR tetramer [^{12}C-^{14}N]:[^{13}C-^{15}N]	Theoretical MW (Da)	Measured MW (Da)
4:0	55570	55581.46 ± 5.10
3:1	56353	56362.61 ± 12.68
2:2	57136	57159.00 ± 14.10
1:3	57919	57935.30 ± 4.38
0:4	58685	58699.32 ± 23.40

Supplementary Table S2. Theoretical and measured molecular masses of TTR tetramers with different numbers of [^{12}C-^{14}N] and [^{13}C-^{15}N] labelled subunits incorporated, observed in Figure 1c.

[holoRBP]/[TTR_4]	$k_{d,mon}$	$k_{d,dim}$	$k_{d,app}$	s.d.
0	6.00×10^{-3}	7.57×10^{-2}	8.17×10^{-2}	1.45×10^{-2}
0.25	3.00×10^{-4}	3.37×10^{-2}	3.40×10^{-2}	3.77×10^{-3}
0.5	3.00×10^{-5}	1.33×10^{-2}	1.33×10^{-2}	1.79×10^{-3}
0.75	2.01×10^{-5}	7.46×10^{-3}	7.48×10^{-3}	1.39×10^{-3}
1	1.80×10^{-5}	4.65×10^{-3}	4.67×10^{-3}	4.31×10^{-3}
2	1.26×10^{-5}	1.84×10^{-3}	1.86×10^{-3}	5.98×10^{-4}

Supplementary Table S3. The apparent disassembly rate constant of TTR_4 depends on the concentration of holoRBP. For each experiment, the decay of homotetrameric TTR was fitted to the model describing subunit exchange to yield monomeric disassembly rate constants ($k_{d,mon}$) and dimeric disassembly rate constants ($k_{d,dim}$). The apparent disassembly rate constants, $k_{d,app}$, were obtained from a sum of $k_{d,mon}$ and $k_{d,dim}$, together with errors reported to one standard deviation. The unit is h^{-1}.

[1] McCammon, M.G. et al. Screening transthyretin amyloid fibril inhibitors: Characterization of novel multiprotein, multiligand complexes by mass spectrometry. *Structure* **10**, 851-863 (2002).